Economic Geology
Vol. 70, 1975, pp. 781–799

Formation of Fractures Around Magmatic Intrusions and Their Role in Ore Localization

H. KOIDE AND S. BHATTACHARJI

Abstract

An exact solution of three-dimensional theory of elasticity in an infinite elastic rock medium around magma reservoirs of various aspect ratios and the criteria of rock fracturing provide an important tool for the interpretation of the origin and nature of distribution of many ore-bearing fracture systems around magmatic bodies in the world. Theoretical analyses suggest the conditions and regions of formation of (1) dominant radial fractures, (2) dominant concentric fractures or combination of radial and concentric fractures, and (3) central subsidence (or graben) in domal uplift related to intrusions of magma bodies of various shapes and sizes. The relations of these fracture systems to the deposition of ore-bearing fluids are discussed in the light of excess magma and hydrothermal fluid pressures. Caldera subsidence and dominant concentric fractures, such as in the San Juan Mountains mining district in Colorado, are, according to our analyses and interpretations, related to intrusion(s) of vertically elongated magma cupolas and high magma and hydrothermal fluid pressures. This differs from Anderson's original contention (1936) that caldera subsidence and outward-dipping ring fractures are due to lower relative magma pressure than lithostatic pressure. Wedging action of magma immediately above a vertically elongated prolate magma body is suggested as a cause of central graben bounded by funnel-shaped normal faults over wide domal uplift. Displacement along normal faults causes underground subsidence above magma cupolas. Extension of such faults close to the surface and displacement along them can produce surface caldera subsidence. Vein-type deposits commonly associated with funnel-shaped felsic (rhyolitic) bodies may be related to near-surface caldera subsidence. The origin of arcuate zones of breccia pipes such as in Silverton cauldron, Colorado, appears to be related to axial symmetric stress condition(s) due to vertically elongated magma body at depth.

Estimation of stress distribution around spheroidal and prolate magma bodies suggests development of possible zonal distribution of fractures from the periphery of the magma outward in the order of (1) continuous tension fracture zone, (2) brittle fault zone, (3) ductile fault zone followed by no fault zone. Brittle fault and continuous tension fracture zones provide excellent sites for ore mineral localization. The zonal distribution of fractures also suggests, in a general way, mode of origin and possible extent of distribution of various fracture types, hydrothermal zoning, and their alterations.

Introduction

IT is generally recognized that a great many primary mineral deposits are concentrated in and around small stocks or cupolas of large batholiths (Emmons, 1933, 1937; Bateman, 1951). Their close relationships have led many to infer that the mineral lode(s) had formed from fluids expelled from such masses. Emmons (1933, 1937, 1940) suggested that wedging by vapor pressure produced vein fractures in the roofs and surrounding hoods of stocks and cupolas. Newhouse (1942), Wisser (1960), and others have shown that structural domes, anticlines, and fractures associated with them, which act as areas of ore localization, are commonly associated with igneous intrusion(s) or plutons. Imai (1966) has noted that many vein-type deposits in Japan are localized in fractures produced by magmatic upwelling or subsidence (including cauldron subsidence) subsequent to the main intrusion magma. It is also known that disseminated porphyry copper deposits are most commonly associated in fractures with igneous stocks or bosses of intermediate to felsic compositions (Emmons, 1940, p. 28). Thus, the fractures which are formed due to intrusion(s) of stocks, bosses, or cupolas of larger igneous masses, or subsequent to magma upheaval and subsidence, act as structural sinks for orebodies. It is, therefore, of great interest to exploration and economic geologists to know the mechanical effects of various magmatic intrusion(s) and the types and patterns of fractures that are produced in the surrounding invaded rocks, which act as hosts for mineralizing solutions and ore fluids. Our primary aim in this

paper is to show, through our theoretical and computerized solutions, the types and patterns of fractures produced due to magmatic intrusion(s) of various sizes and shapes (determined by various aspect ratios) and their similarities with ore-bearing fractures associated with magmatic intrusions in many important mining districts. This enables prediction of the general form and dimensions of magmatic intrusions from the nature of superficial fracture patterns, and the general extent of ore-bearing fractures associated with bodies of various dimensions, thus facilitating exploration of ore deposits.

We also discuss and interpret the development of various fracture patterns and the significance of these for structural control of ore deposits from the viewpoints of rock mechanics and the theory of fractures in rocks.

Previous work

In his classic work, Anderson (1936) presented a mechanical theory for the formation of cone sheets and ring dikes by magmatic intrusion. This work provided a theoretical basis for later study on fracture patterns, although in his analysis he assumed a "point push" rather than a magma reservoir pressure. Anderson (1938, 1951) pointed out that extension fractures occur in a plane normal to the direction of maximum principal stress (i.e., to the direction of minimum compression) by the wedging action of the magma intrusion. He concluded that the cone sheets fill extension fractures formed by the magma pressure exceeding the lithostatic pressure, and the ring dikes occupy shear fractures formed when the magma pressure was less than the lithostatic pressure. Odé (1957) analyzed the effects of horizontal nonhydrostatic stress on radial fractures around a cylindrical magma reservoir. Garson (1959), in his analysis, assumed a circular area of upward pressure and obtained fracture patterns similar to those predicted by Anderson's theory. Onda (1960) analyzed the collapse of rocks due to a circular empty magma reservoir. He concluded that the collapse hypothesis might not explain the mechanism of calderas of dimensions smaller than 20 km, and that eruptive explosions may have played a dominant role in the formation of small calderas. Robson and Barr (1964) studied the effects of nonhydrostatic tectonic stress on a circular-shaped magma chamber. Their study showed that calderas were formed under tectonic horizontal extension (and the minimum diameter of caldera should be in the order of 4 km). Their interpretation that the ring dikes filled up extension fractures and cone sheets filled up shear fractures is contrary to Anderson's view. Photoelastic experiments by Durrance (1967) supported Robson and Barr's interpretation. However, a more recent analysis by Roberts (1970), using the same solution as Robson and Barr (1964) but including the effect of pore solution pressure (in addition to magma pressure), pointed to a very different conclusion: the cone sheets and ring dikes occupy tension fractures formed under excess magma pressure, while some other ring dikes occupy shear fractures under reduced magma pressure.

Conflicting interpretations of these kinds are due not only to the lack of exact knowledge about the three-dimensional structure of the dikes but also to incomplete mechanical analyses. Although some (Anderson, 1936, Robson and Barr, 1964, etc.) have discussed three-dimensional fracture patterns, their discussions have been based essentially on two-dimensional analyses. In addition, simple geometric forms, such as point(s), line(s), circular holes, etc., were assumed for magma bodies. Unfortunately, in nature such perfect geometry is rarely encountered. As fractures are formed under high stress concentration, the shape of the apex of the magma reservoir which controls the stress concentration is especially important for any realistic theoretical solution for fracture development due to magmatic intrusion. In the present study, we have considered the curvature of the apex of the magmatic intrusion(s) of various aspect ratios for the analyses of fracture patterns developed in the surrounding rocks, by using a three-dimensional theory of elasticity (Bhattacharji and Koide, 1974).

Methods of analysis

An isolated prolate magma chamber is assumed to exist in an isotropic, homogeneous, elastic rock body (Fig. 1). A three-dimensional exact solution of theory of elasticity has been obtained on the basis that hydrostatic magma pressure acts across the wall of the magma reservoir. As magmas (particularly the felsic types with which many ore deposits are associated) are generally lighter than the surrounding rocks in the deeper level of the crust, the effective stress[1] $(\sigma - P)$ is maximum at the top of the magma reservoir.

As fractures also occur in the areas of largest effective stress (as discussed later), magma reservoirs tend to develop upward (Koide, 1974; Mogi, 1974). Thus, a vertically elongated magma reservoir is generally expected to form at the deeper

[1] To avoid confusion, we have considered tensile stress as positive and effective pressure as negative. The maximum effective stress is considered to be synonymous with minimum effective compressive stress or minimum value of effective pressure.

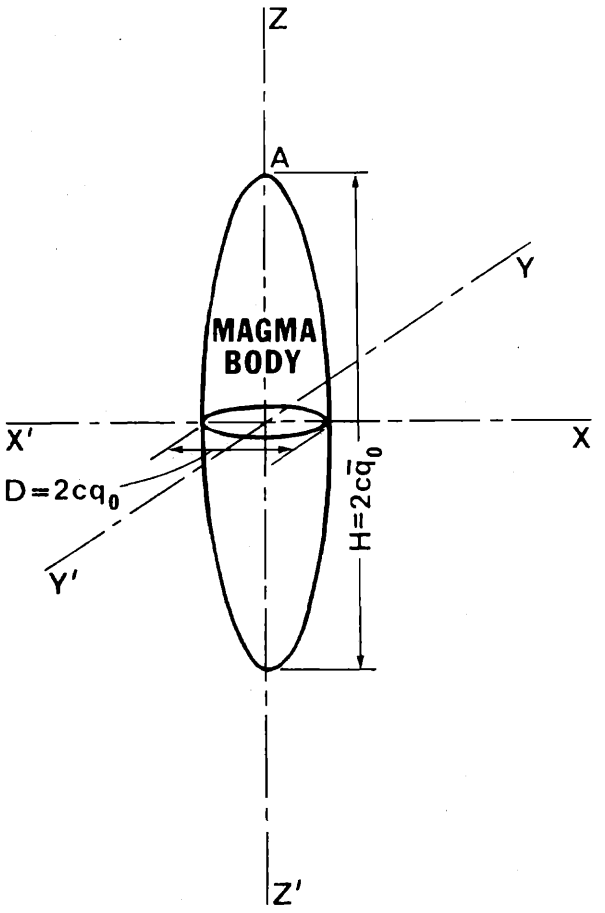

FIG. 1. Diagrammatic representation of prolate magma body and its coordinate system.

level of the lithosphere. Because of this, we have assumed the magma reservoir to be an elongated spheroid, whose vertical section (with the long axis) is an ellipse and the horizontal section a circle (Fig. 1). As the shape of the upper part of the magma reservoir affects the stress concentration primarily around its apex, the vertical prolate magma reservoir represents the shape of an actual stock or a cupola more realistically than the circular shape of the magma reservoir. Homogeneous isotropic lithostatic stress is assumed when there is no effect of magma pressure (i.e., stress is homogeneous and isotropic infinitely far from the magmatic source). This assumption is valid, as actual field measurements of stresses have shown them to be nearly isotropic, and horizontal stresses were found to be almost equal to the overburden rock pressure (Suzuki et al., 1967; Hast, 1973). As magma pressure and horizontal confining stress affect stress concentration primarily around the apex of a magma reservoir, isotropic lithostatic stress is applicable as a first approximation. The effects of gravity force, earth's surface, anisotropy, inelasticity, etc., are neglected in our analyses. Despite these limitations, the results presented below appear to be consistent with natural occurrences. Although numerical calculations can supplement some of the weaknesses of the analytical method, a complete numerical solution is still difficult to obtain by a finite element method. Some combination of analytical and numerical methods may prove more fruitful for future study.

Solution for Elastic Stress Distribution around a Magma Reservoir

Using Boussinesq's three-function method, Sadowski and Sternberg (1947, 1949) and Edwards (1951) obtained an exact solution for the distribution of stress around a prolate cavity in an infinite, homogenous, isotropic elastic body which is considered to be in an arbitrary uniform state of stress at an infinite distance from the cavity. Koide (1968, 1970, 1972) further developed Edwards' solution into a more convenient form for calculation and applied the solution for the study of development of fractures. Stress distribution around spheroidal magma reservoir was obtained by using a solution following Koide's modified equation (1972). Only a part of the theoretical solution relevant to this study is described here.

A cartesian coordinate is determined in a manner such that the origin of the coordinate is in the center of the magma reservoir and the Z-axis coincides with the longest (vertical) axis (of rotation) of prolate magma body (Fig. 1). A prolate spheroidal coordinate is taken as follows:

$$\left.\begin{aligned} X &= C\cdot\sinh\alpha\cdot\sin\beta\cdot\cos\gamma = C\cdot q\cdot p\cdot\cos\gamma \\ Y &= C\cdot\sinh\alpha\cdot\sin\beta\cdot\sin\gamma = C\cdot q\cdot p\cdot\sin\gamma \\ Z &= C\cdot\cosh\alpha\cdot\cos\beta = C\cdot\bar{q}\cdot\bar{p} \end{aligned}\right\} \quad (1)$$

where

$$q = \sinh\alpha, \quad \bar{q} = \cosh\alpha = \sqrt{1+q^2},$$
$$p = \sin\beta, \quad \bar{p} = \cos\beta = \sqrt{1-p^2}.$$

When $q = q_0$ and $\bar{q}_0 = \bar{q}_0$ at the wall of the prolate magma reservoir, the longest diameter of the reservoir along the Z-axis, $H = 2C\bar{q}_0$, and the shortest diameter perpendicular to the Z-axis, $D = 2Cq_0$.

Stresses at any point in the surrounding rock body are expressed as σ_α, σ_β, σ_γ, $\tau_{\alpha\beta}$, $\tau_{\beta\gamma}$, $\tau_{\gamma\alpha}$ along the spheroidal coordinate. σ_α is the normal stress which acts parallel to the α-axis of the prolate spheroidal coordinate. $\tau_{\alpha\beta}$ is the tangential stress

which acts along the plane normal to the direction of α-axis and parallel to the β-axis or vice versa. σ_α is the stress normal to the wall of the magma reservoir. Then the boundary condition is $\sigma_\alpha = P$, $\tau_{\alpha\beta} = \tau_{\beta\gamma} = 0$ at $q = q_0$, where P = magma pressure. We also assumed isotropic lithostatic stress ($\sigma_\alpha = \sigma_\beta = \sigma_\gamma = \sigma_1$; and $\tau_{\alpha\beta} = \tau_{\beta\gamma} = \tau_{\gamma\alpha} = 0$ where σ_1 = lithostatic stress).

At an arbitrary point in the surrounding rock, stresses are obtained as follows:

$$\left.\begin{aligned}
\sigma_\alpha &= \sigma_1 + \{a_{1h}S_{1\alpha} + a_{2h}S_{2\alpha} + (q^2 - q_0^2)a_{1h}S_{3\alpha}\}\cdot(\sigma_1 - P)/D_1 \\
\sigma_\beta &= \sigma_1 + \{a_{1h}S_{1\beta} + a_{2h}S_{2\beta} + (q^2 - q_0^2)a_{1h}S_{3\beta}\}\cdot(\sigma_1 - P)/D_1 \\
\sigma_\gamma &= \sigma_1 + \{a_{1h}S_{1\gamma} + a_{2h}S_{2\gamma} + (q^2 - q_0^2)a_{1h}S_{3\gamma}\}\cdot(\sigma_1 - P)/D_1 \\
\tau_{\alpha\beta} &= \sigma_1 + \{a_{1h}S_{1\alpha\beta} + a_{2h}S_{2\alpha\beta} + (q^2 - q_0^2)a_{1h}S_{3\alpha\beta}\}\cdot(\sigma_1 - P)/D_1 \\
\tau_{\beta\gamma} &= \tau_{\gamma\alpha} = 0
\end{aligned}\right\} \quad (2)$$

where ν = Poisson's ratio of surrounding rocks

$$h = 1/\sqrt{q^2 + p^2},\quad Q = 1 - \bar{q}\cdot\coth^{-1}\bar{q},\quad h_0 = 1/\sqrt{q_0^2 + p^2},\quad Q_0 = 1 - \bar{q}_0\cdot\coth^{-1}\bar{q}_0,$$

$$D_1 = 4\{-(1+\nu)q_0^4Q_0^2 + q_0^3Q_0[2(1-\nu) + 3q_0^2] + 1 - \nu + q_0^2\}/\bar{q}_0q_0^2,$$

$$a_{1h} = -2(3q_0^2Q_0 + 1),\quad a_{2h} = 2[(1+\nu)q_0^2Q_0 + \nu],$$

$$S_{1\alpha} = -(1+\nu)\bar{q}(1 + q^2Q)/q^2 + 3\bar{q}/q^2 + h^2q[\nu + (1+\nu)q^2Q],$$

$$S_{1\beta} = (1+\nu)(1 + q^2Q)/\bar{q} - h^2\bar{q}[2 + \nu + (1+\nu)q^2Q],$$

$$S_{1\gamma} = [-2 + \nu - (1-2\nu)q^2]/q^2\bar{q} - (1+\nu)Q/\bar{q} - 2\nu h^2,\bar{q}$$

$$S_{1\alpha\beta} = -h^2p\bar{p}[\nu + (1+\nu)q^2Q]/q,$$

$$S_{2\alpha} = (1 - q^2)/q^2\bar{q} - (1 + 3q^2)Q/\bar{q} + h^2\bar{q}(1 + 3q^2Q),$$

$$S_{2\beta} = 1/\bar{q} + (2 + 3q^2)Q/\bar{q} - h^2\bar{q}(1 + 3q^2Q),$$

$$S_{2\gamma} = -1/q^2\bar{q} - Q/\bar{q},\quad S_{2\alpha\beta} = -h^2p\bar{p}(1 + 3q^2Q)/q,$$

$$S_{3\alpha} = -h^2\bar{q}/q^2 - h^4\bar{q},\quad S_{3\beta} = h^4\bar{q},\quad S_{3\gamma} = h^2\bar{q}/q^2,$$

$$S_{3\alpha\beta} = -h^4p\bar{p}/q.$$

Stress Distribution around a Magma Reservoir

Stress distributions around prolate magma bodies of aspect ratios (D:H) as 1:1.4, 1:10, and 1:100 have been calculated using Equation (2). In Figure 2, stress distributions are shown in the radial (vertical) plane which contains the Z-axis of rotation of a prolate magma body. If the body is vertical, the indicated radial plane is also vertical. As the shape of the magma body and boundary condition(s) are axially symmetric, total stress distribution is also axially symmetric; thus stress distribution can be represented in a radial plane. In Equation (2), the direction of σ_γ is normal to the radial plane. As $\tau_{\beta\gamma} = \tau_{\gamma\alpha} = 0$, σ_γ is one of the principal stresses, as the two other principal stresses (σ_1 and σ_2) are determined by σ_α, σ_β, and $\tau_{\alpha\beta}$, the directions of which lie within the radial plane.

Contours in Figures 2A, C, E denote maximum tensile stress (σ_1 kb) within the radial plane, when the excess magma pressure ($\Delta P = P - \sigma_1$) is -1 kb and lithostatic stress (σ_1) is negligible. The value(s) of maximum stress within the radial plane under conditions of general lithostatic stress can be obtained from the value(s) of stress in Figure 2 as follows:

$$\sigma_1(\text{general}) = \sigma_1 + (\sigma_1 - P)\sigma_1(\Delta P = -1) \quad (3)$$

The directions of σ_2 are indicated by short straight lines in Figure 2. The contours in Figures 2B, D, F denote the maximum shearing stress within the radial plane $\tau_m = (\sigma_1 - \sigma_2)/2$, when the excess magma pressure (ΔP) is -1 kb. The value(s) of maximum shearing stress within the radial plane under general lithostatic stress conditions can be obtained from the value(s) in Figure 2 as follows:

$$\tau_m(\text{general}) = (\sigma_1 - P)\tau_m(\Delta P = -1) \quad (4)$$

Case I. Stress distribution around a near-spherical magma body

The magma reservoir of aspect ratio 1:1.4 is nearly spherical in shape (Fig. 2). Contours are also nearly circular, but stress is higher around the apical area. The highest tensile stress -0.738 kb occurs in the surrounding rocks just above the

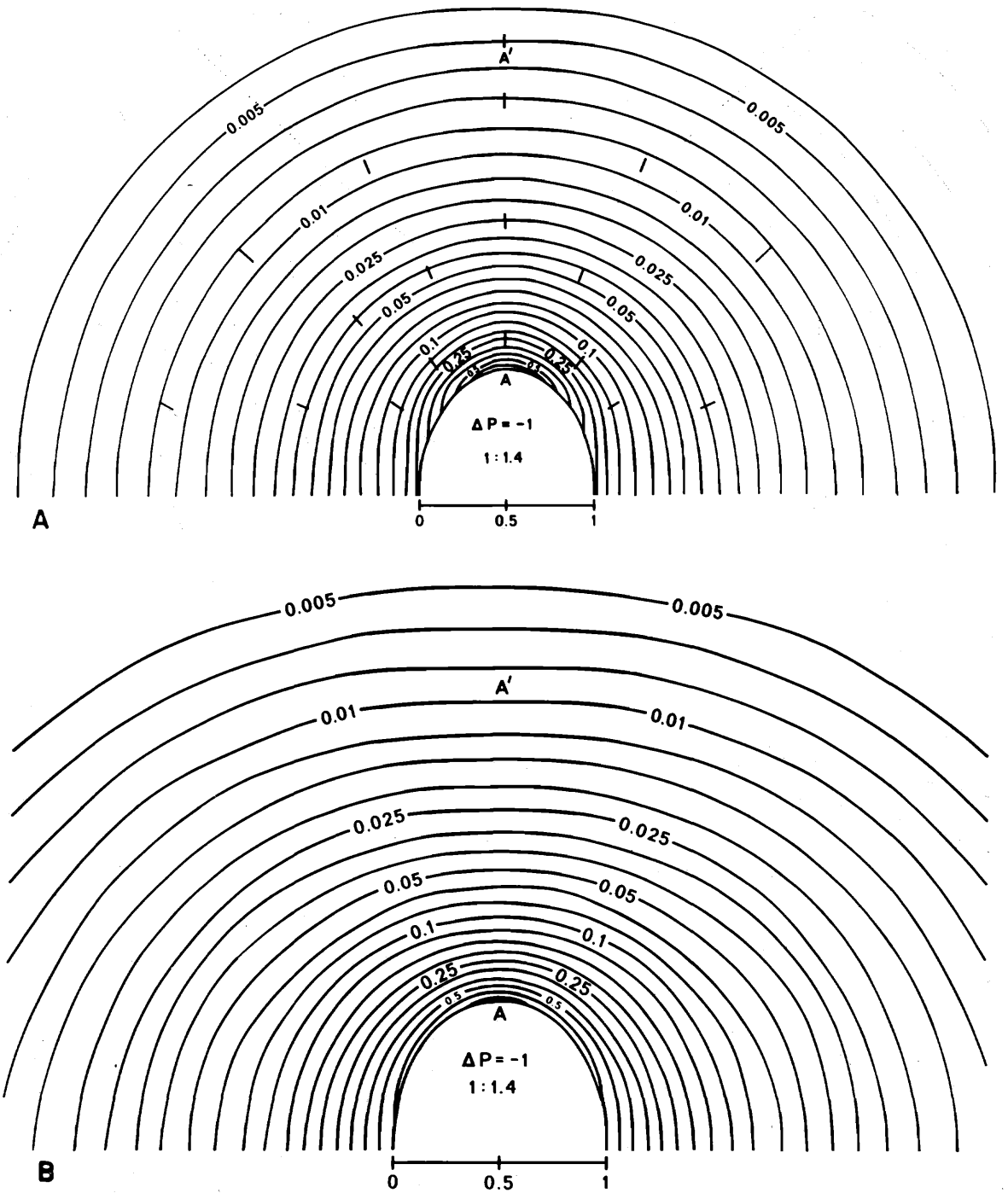

FIG. 2. Contour diagrams (in kb) in radial (vertical) section around prolate magma reservoirs of stress concentration, due to excess magma pressure ($\Delta p = P - \sigma_1 = -1$ kb). Only the contours around the apex of the magma body are shown in Figures A to E. The minimum diameter of the magma reservoir is indicated as unit length. The stress components parallel to the radial section are shown in Figures A to E. The uniform lithostatic stress is neglected. All normal stresses are tensile within the funnel-shaped surface (V.T.) in Figures C and E when lithostatic stress is zero. Short straight lines in A, C, and E indicate the directions of the minimum stress (σ_2) parallel to the radial section. Poisson's ratio $\nu = 0.3$.

A. Maximum stress (σ_1) parallel to the radial section around a magma reservoir of aspect ratio 1:1.4.
B. Maximum shearing stress (τ_m) parallel to the radial section around a magma reservoir of aspect ratio 1:1.4.

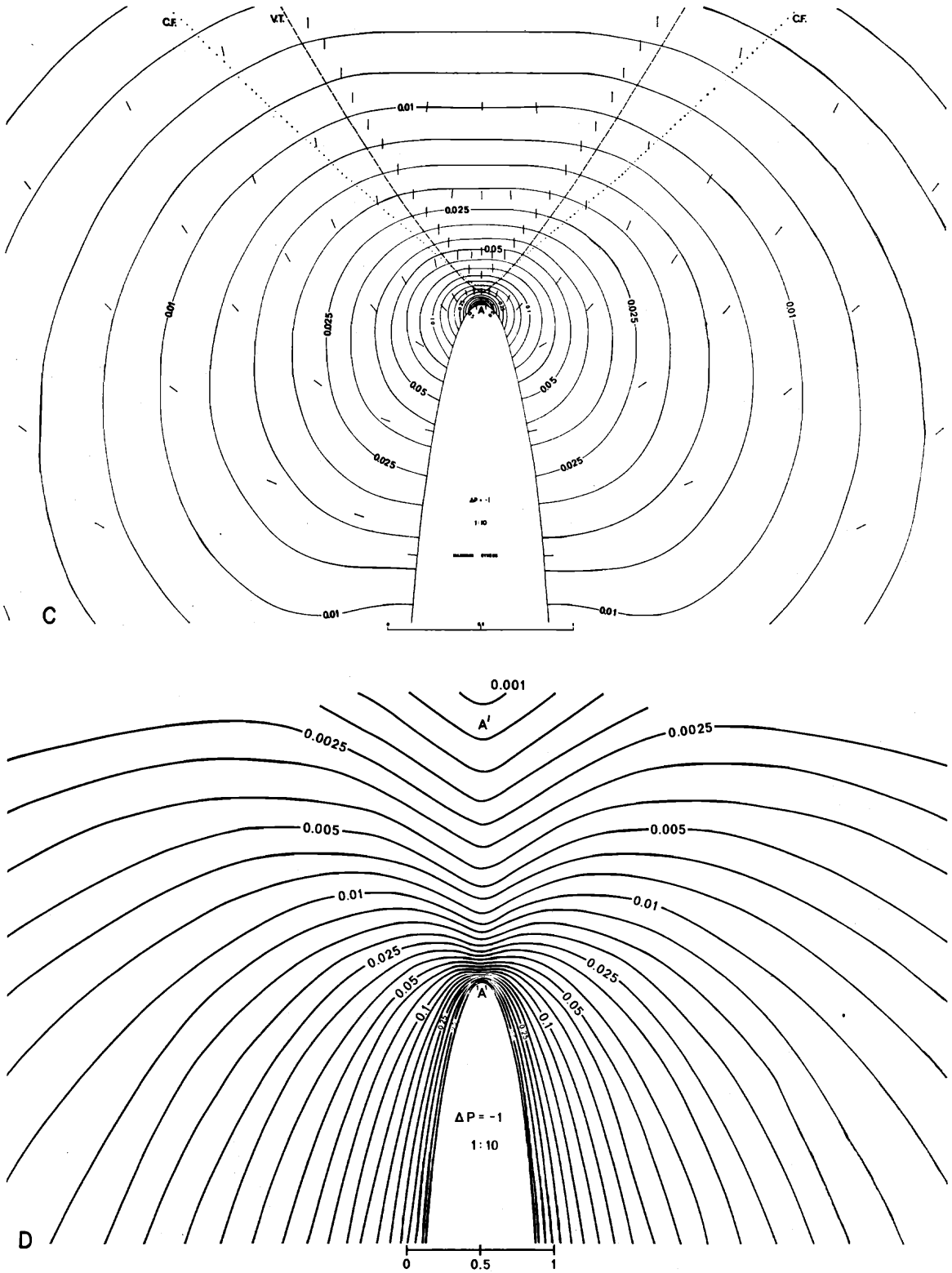

C. Maximum stress (σ_1) parallel to the radial section around a magma reservoir of aspect ratio 1:10.
D. Maximum shearing stress (τ_m) parallel to the radial section around a magma reservoir of aspect ratio 1:10.

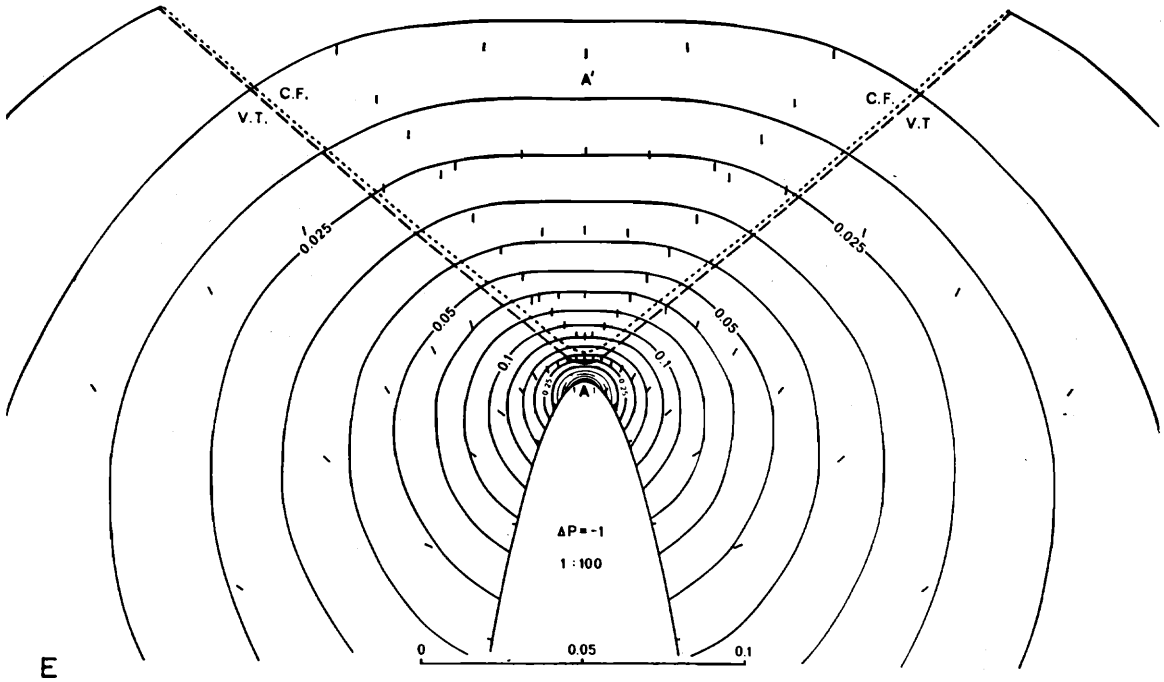

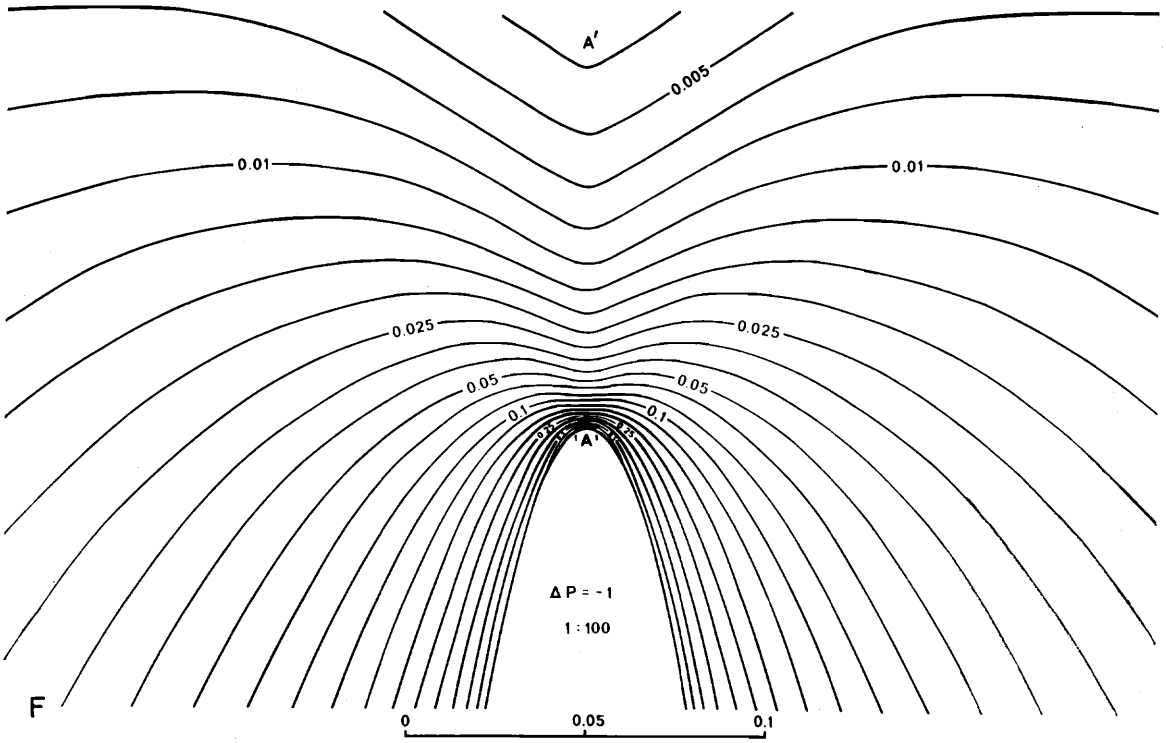

E. Maximum stress (σ_1) parallel to the radial section around a vertically elongated prolate magma body of aspect ratio 1:100.

F. Maximum shearing stress (τ_m) parallel to the radial section around a vertically elongated prolate magma body of aspect ratio 1:100.

apex of the magma reservoir (A). The pattern of stress direction(s) of σ_2 are almost radial. At the wall of the magma reservoir, the direction of σ_2 is normal to the wall and the value of σ_2 is always -1 kb. The highest shearing stress 0.869 kb occurs at the apex of the magma reservoir. As a general rule, if the shape of the magma reservior is spherical, contours for stress distribution will be circular, and the pattern(s) of stress directions of σ_2 will be radial. In nature a vertically elongated magma body (the cases we have considered for our analyses, such as 1:1.4) is more a realistic shape than a sphere. Piecemeal stoping above an emplaced magma body, in addition to higher effective stress, would tend to make even a spherical magma reservoir into an elongated, prolate spheroid. It is noteworthy that the stress pattern(s) around a near-spherical magma body (aspect ratio 1:1.4) is comparable to the stress pattern(s) obtained by Anderson (1936) for a magma body of similar shape. In Figure 3A, stress distribution around a prolate magma reservoir of aspect ratio 1:1.4 is shown under the lithostatic pressure of -1 kb. The lithostatic pressure of -1 kb corresponds to the overburden rock pressure of roughly the depth of 4 km. Although the exact depth of intrusion of magma at the time of fracturing and emplacement of orebodies is impossible to determine, the field evidence indicates that most of the intrusives, around which there are important orebodies, probably crystallized at depths greater than 1.5 km (Bateman, 1951, p. 88). Gilluly (1946) estimated the depth of crystallization of Cornelia quartz monzonite, acting as a host for the porphyry copper deposit of Ajo, Arizona, to be 1 to 3.3 km. Ishihara's (1967) estimation for the Questa, New Mexico, molybdenum deposit, is 1 to 1.6 km. Yokoyama (1971, 1974) estimated the depth of magmatic intrusion, in areas of major volcanic activity, to be in the order of 2 to 6 km (average of 4 km) from his study of crustal movement during volcanic activity. It is interesting to note that the depth of 4 km corresponds to -1 kb lithostatic pressure, and approximates the depth of formation of mesothermal ore deposits ($\approx$1.7 to 6.7 km) (Ridge, 1968). Recently, Aramaki (1971) has shown from his hydrothermal experiments the stability of coexisting minerals (quartz, plagioclase, etc.), liquid, and gas phases in the range of magma pressure of 1.6 to 1.9 kb for materials of composition of pumice from Aira Caldera, Japan. Roberts (1970) has also suggested an excess magma pressure (i.e., $\Delta P = P - \sigma_1$) to be about -1 kb for basaltic magma at a depth of 5 to 10 km. Thus, the examples we have presented here, namely, intrusion of vertically elongated prolate magma bodies of various aspect ratios (1:1.4, 1:10, etc.), stress distribution in elastic rocks, and development of probable fracture patterns in the surrounding country rocks (in which ore mineral concentrates) due to an excess magma pressure (Fig. 3), are more natural and applicable to a wide range of cases as well as to mesothermal ore deposits associated with igneous intrusion(s).

Case II. Stress distribution around a magma body with increasing aspect ratio

As we pointed out earlier, the size, shape, and depth of intrusion of magma bodies vary greatly in nature and are hard to estimate. A magma reservoir, due to higher effective (tectonic) stress, piecemeal and convective stoping (Bhattacharji and Schleifer, 1970), could grow progressively, vertically, in situ even after emplacement. Therefore, it is important to consider the effects of intrusions of magma bodies of various or increasing aspect ratios which may cause different stress distributions in the surrounding country rock(s). This variation may produce different and new fracture patterns, or may influence previous fracture patterns, thus affecting the localization of ore minerals. Here we are presenting the summary of the results of our analysis of vertical prolate magma bodies of aspect ratios 1:10 and 1:100 (Figs. 2C-F). One could consider the results of our analyses for stress distribution and fracture patterns due to individual, discrete magma bodies of different aspect ratios, or due to a magma body of progressively increasing aspect ratio from 1:10 to 1:100 in the vertical direction of intrusion.

Near the apex of magma reservoirs, stress contours are almost arcuate, and directions of σ_2 dip inward or are vertical along the extension of the central axis of the magma reservoir. Patterns of stress distribution near the apex of elongated magma reservoirs of aspect ratios 1:10 and 1:100 are similar to that of a near-spherical magma body of aspect ratio 1:1.4, although stress concentration is much higher (Fig. 2). At the apex of a magma reservoir of aspect ratio 1:10, the highest maximum tensile and shearing stresses are 1.379 and 1.191 kb, respectively, while for a body of aspect ratio 1:100, they are 1.428 kb (tensile stress) and 1.214 kb (shearing stress). Inside a funnel-shaped surface in Figures 2C, E, far above the magma reservoirs, the contours for σ_1 are slightly concave upward; while the upward concavity of contours for τ_m is more apparent in Figures 2D, F. Directions of σ_2 are vertical along the central axis of the magma reservoir and along a funnel-shaped surface (Figs. 2C, E). On plan view, the funnel-shaped surface

appears circular because it is axially symmetric. σ_2-directions dip inward outside the funnel-shaped fracture surface and dip outward at steep angles inside it (Figs. 2C, E). The dip of the upwardly concave funnel-shaped surface varies with height (with the vertical direction of σ_2), but the average dip angles of 58° and 50° with the vertical stress (σ_2) axis for the funnel-shaped fracture surface are estimated for magma bodies of aspect ratios 1:10 and 1:100, respectively. The stress (σ) is three-dimensionally tensile inside the funnel-shaped surface (V.T. in Figs. 2C, E). The funnel-shaped surface (V.T.) dips inward at angles of about 55° and 40° for magma bodies of aspect ratios 1:10 and 1:100, respectively. The occurrence of a tensile zone above a magma reservoir due to intrusive pressure of magma may appear paradoxical. However, the wall of a vertically elongated magma reservoir has a force component that is larger horizontally than vertically. This will tend to enlarge the magma reservoir in the lateral direction, thereby producing tensile stress instead of compressive stress in the surrounding rock at the apical zone of the magma reservoir; this would produce wedging action more readily than lifting its top. This horizontal extension in and around a deeper level magma reservoir produces a three-dimensional extension above it. Therefore, for a more elongated magma reservoir of aspect ratio 1:100, there will be a greater tendency for extension inside the funnel-shaped surface (above the magma reservoir), although the patterns of stress concentration for bodies of aspect ratios 1:10 and 1:100 are very similar. The similarity of stress concentration (Figs. 2C–E) is due to the similarity of shapes of the apex of magma reservoirs of aspect ratios 1:10 and 1:100. It is to be noted, however, that for magma reservoirs of aspect ratio less than 1:10 the extent of the area of stress concentration is approximately proportional to the radius of curvature of the apex of slender, prolate magma reservoirs. It is also noteworthy that in a vertically elongated magma reservoir, lithostatic stress, magma pressure, and effective stress can change (or vary) with depth. Thus, a general buildup of magma pressure would lead to horizontal stretching of the magma reservoir, resulting in extension into the rock(s) above it and concomitant wedging (and intrusion) of magma.

The principal stress (σ_γ) for a prolate magma reservoir of aspect ratio 1:100 (acting perpendicular to the radial plane) is shown in Figure 3 by broken lines. Here the principal stress σ_γ, outside the funnel-shaped fracture surface (C.F.), is higher than the maximum stress σ_1 acting within the radial plane; in this respect it is similar to near-spherical magma bodies of aspect ratio 1:1.4 (Fig. 3). However, inside the funnel-shaped fractured surface (C.F.), σ_γ is higher than σ_1. The values of σ_1 and σ_γ are equal along the (vertical) central axis of magma reservoir and along the funnel-shaped surface (C.F.). The stress analyses presented here (Fig. 3) are most applicable to cases due to magma bodies of small diameter, although they could be applied to approximate estimation of stress distributions and possible fracture patterns in country rocks due to large magma reservoirs.

Criteria for Modes of Fracturing and Effects of Interstitial Fluid Pressure on Fracturing

Fracture openings provide passage for the easy migration of hydrothermal fluids and sites for ore mineral deposition; the patterns of the fractures, however, control the structure of the ore-bodies. Probable stress distributions around magma bodies discussed so far indicate only likely fracture patterns. However, whether such fracturing would actually occur and ore minerals would concentrate there would depend largely on the condition of stress. Hence, a short summary of the criteria of fracturing would help our discussion on ore mineral deposition in various types of fractures.

Robson and Barr (1964) assumed the Coulomb-Navier criterion from shear fracture, and Roberts (1970) used the Griffith theory for determining the conditions of fracturing. The Griffith theory is applicable to brittle fracturing and indicates how fractures propagate. However, Griffith cracks which, in Griffith theory, are assumed to pre-exist before fracturing, generally close under high compressive stress (Koide, 1968, 1972). In our analysis, we have recognized three probable types (or zones) of fracturing. Occurrence and continuity of tension fractures in the immediate vicinity of the periphery of the magma reservoir is possible when effective tensile stress is higher than critical tensile stress. Critical tensile stress is usually very small under natural conditions in a large rock body, as such a rock may contain numerous planes of weakness which act as distinct Griffith cracks under effective tensile stress. If we assume critical tensile stress to be practically zero, continuous tension fractures can occur under the following condition:

$$\sigma - p > 0 \qquad (5)$$

The occurrence of a brittle fault zone succeeding tensile fracture would indicate the propagation of Griffith cracks under compressive stress. Therefore, they are predominantly tensile fractures. The continuation of the opening of such fractures under

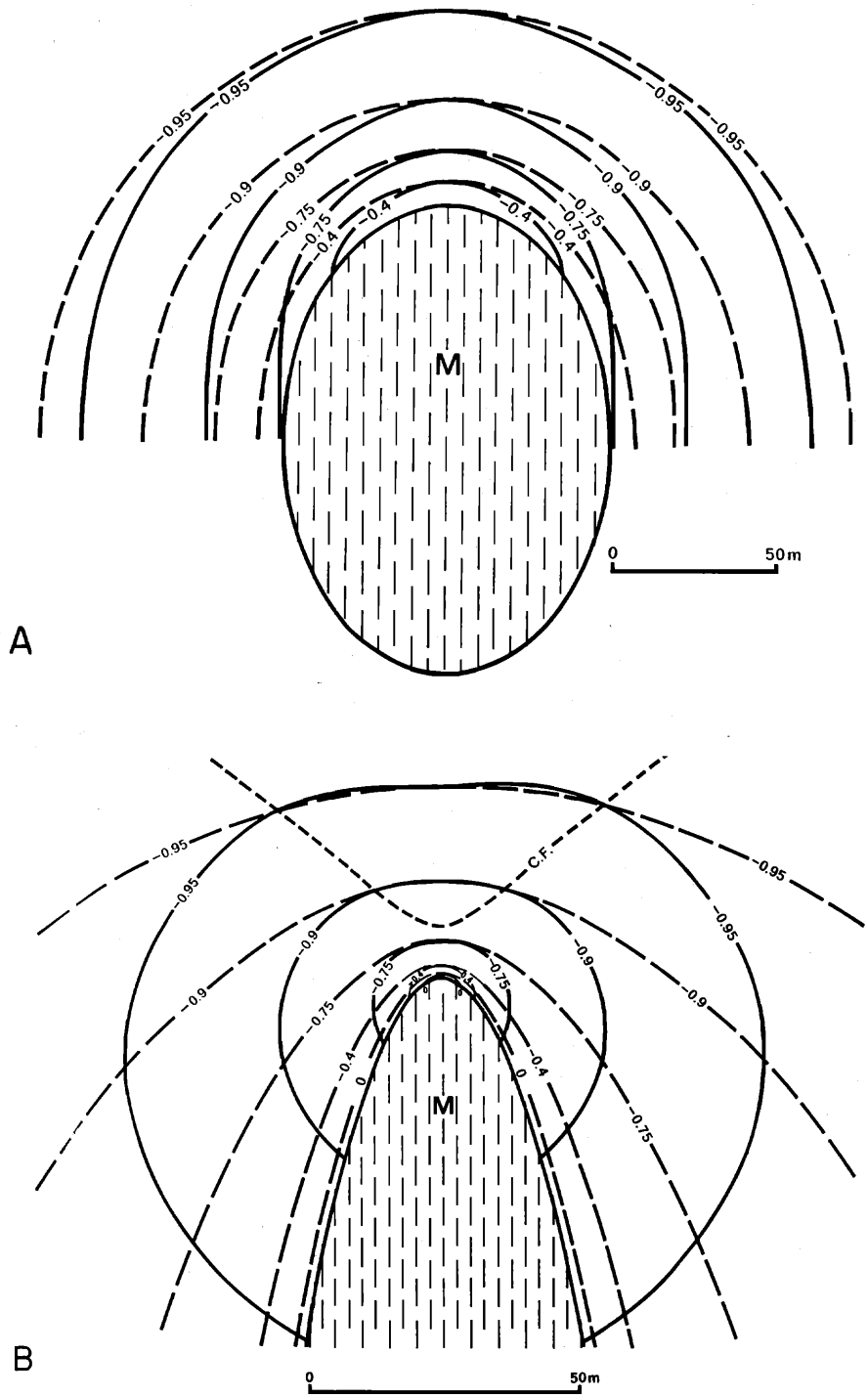

FIG. 3. Stress distribution around small prolate magma reservoirs due to magma pressure of -2 kb at the apex and lithostatic stress of -1 kb (corresponding to pressure at a depth of 4 km). Solid lines indicate contours for maximum stress (σ_1) parallel to the radial section, and broken lines indicate contours for the principal stress (σ_γ) perpendicular to it. The unit of scale is arbitrary.

A. Near-spherical magma reservoir of aspect ratio 1:1.4.
B. Vertically elongated prolate magma reservoir of aspect ratio 1:100. Within the funnel-shaped surface (C.F.) the maximum stress (σ_1) is higher than principal stress (σ_γ).

compressive stress can be understood because a local field of tensile stress develops due to stress concentration near the tips of the Griffith cracks induced by shearing stress (Griffith, 1925). Extension and propagation of Griffith cracks can only occur under high shearing stress when:

$$\tau > -\mu(\sigma - p) \cdots (\sigma - p < 0) \qquad (6)$$

where

$$\mu = \frac{(2-\nu)(1-\nu)}{2G}\sqrt{1 + \frac{2G}{T_m(1-\nu)}},$$

ν is Poisson's ratio, G is rigidity, and T_m is ideal tensile strength of the rock (Koide, 1972; Koide et al., 1974).

Under high compressive stress, if the shearing stress (τ) that develops is lower than that indicated by the criteria of Equation (6), microfractures originate from grain boundaries or various planes of weakness instead of open Griffith cracks. Such a system of microfractures may be called ductile faults. However, such faults are not important in this study as they are not continuously open fractures. A "no fracture zone" which appears adjacent to and outside of the brittle fault zone at shallow depth has no significance for ore mineral localization.

Continuous tensile fractures generally provide a good passage for magmas as well as for hydrothermal fluids. However, small, discontinuous tensile fractures formed under compressive stress from Griffith cracks or planes of weakness can align themselves in en echelon pattern to form a shear fault zone in a later stage of deformation (Koide, 1971). The brittle fault zone is composed predominantly of tensile fractures; however, shear fractures may also form in this zone. The opening of this fault zone at the outer rim of the magma reservoir makes an excellent site for the localization of hydrothermal solutions.

In deformed rocks, with intense fracturing and increasing dilatancy, porosity and permeability increase greatly when the interstitial fluid pressure approaches that of the lithostatic pressure; that is, when the effective stress is almost zero (Handin et al., 1963). In general, interstitial hydrothermal fluids find easier and more permeable passage in continuous tension fractures and less in the brittle fault zone. Magma, on the other hand, can penetrate only continuous tension fractures and wide-open brittle fracture zones when they become directly connected with the magma reservoir at the late phase of fracturing. At shallow depths, interstitial hydrothermal fluid pressure is ordinarily equal to the overburden pressure of ground-water column.

However, interstitial hydrothermal fluid pressure may approach lithostatic pressure under impermeable cap rock (Hubbert and Rubey, 1959; Roberts, 1972). During the intrusion of magma, interstitial hydrothermal fluid pressure may build up by such processes as (1) compression of released superheated or hydrothermal fluid during intrusion of magma, (2) expansion of ground water with rising temperature in sealed water reservoir, (3) emanation of high pressure juvenile hydrothermal fluids from magma, and (4) difference of specific gravity between high temperature hydrothermal fluid and low temperature ground water or host rocks. The last two processes seem to be more important in the upper part of the crust because of the predominance of convective circulation of meteoritic water around shallow igneous stocks (White, 1968; Sheppard et al., 1969; Taylor, 1971). Due to high temperatures in the vicinity of magma pools, upward flow and strong circulation of low density hydrothermal fluid could be a dominant mechanism. In this circulation process, if ground water flows down at the periphery of a magma body and attains a temperature higher than 550°C (Taylor, 1971), the resultant upward-moving low density hydrothermal fluids can easily attain a pressure almost equal to lithostatic pressure. Hence, for our analytical models, 90 percent hydrothermal fluid pressure around magma reservoirs is assumed.

Possible Fracture Patterns around a Prolate Magma Body

Stress distribution around a small prolate magma reservoir of aspect ratios of 1:1.4 and 1:100 in a depth of about 4 km is shown in Figure 3. Here the ratio of magma pressure to lithostatic stress is 2:1 (i.e., −2 kb: −1 kb), and an average interstitial hydrothermal pressure of −0.9 kb around the magma reservoir is assumed.

The zonal distribution of fractures around such magma bodies is obtained by using the nature of stress distribution and the criteria for the mode of fracturing; it is shown in Figure 4. If the Griffith cracks or planes of weakness distribute themselves in all directions, the criteria for mode of fracturing may also be applied for all directions. In Figure 4, the solid lines labeled EO indicate the boundaries along which the effective stress is zero in the direction of maximum stress within the radial plane. The broken lines labeled EO′ indicate the boundaries along which effective stress is zero perpendicular to the radial plane. The solid and broken lines labeled B or B′ are boundaries for brittle faults as established following Equation (6). Continuous radial tension fractures, parallel to the radial plane (i.e., the plane of figure), occur in regions labeled

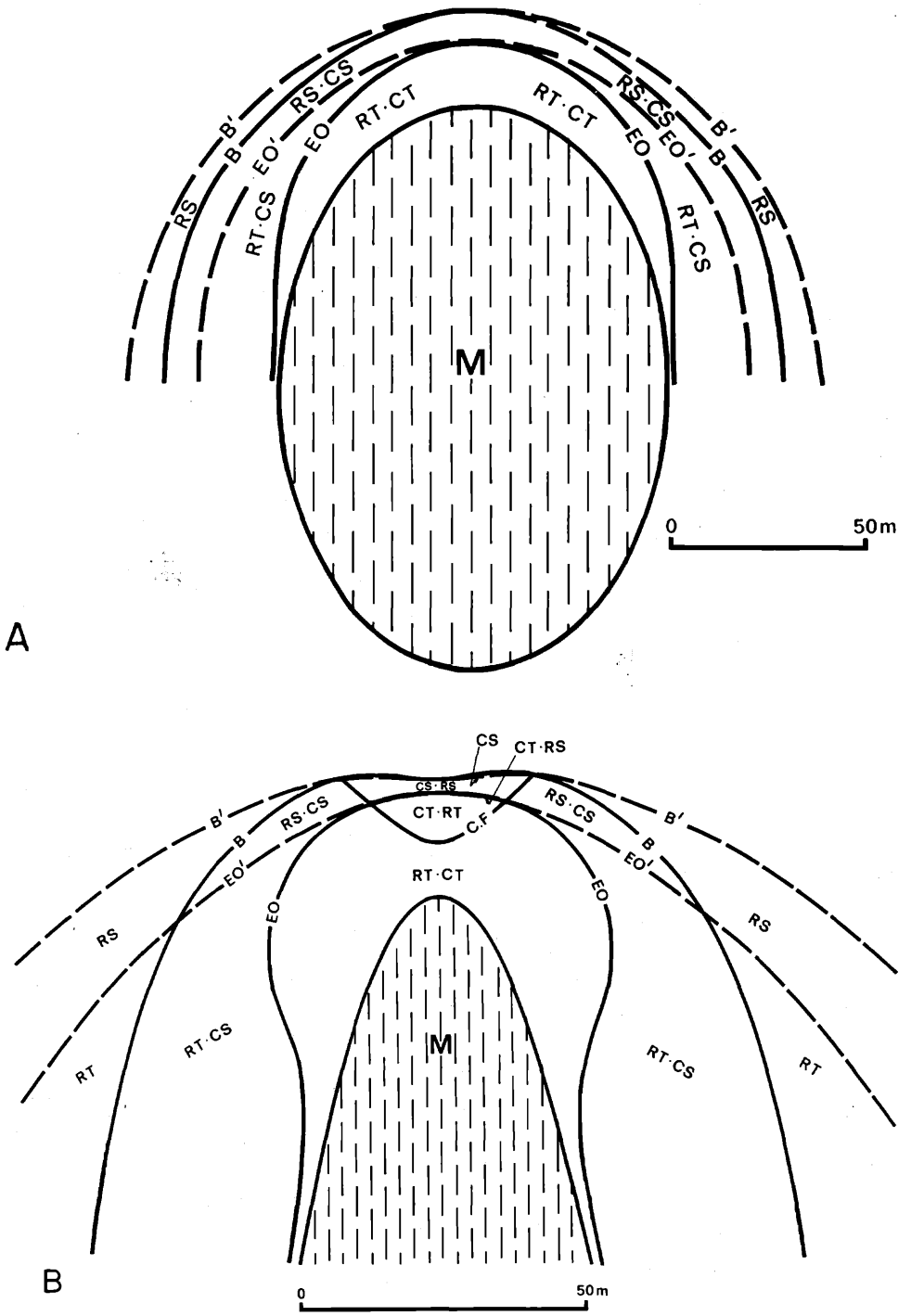

FIG. 4. Diagrammatic sketch for zonal distribution of modes of fractures around a prolate magma reservoir (for magma pressure −2 kb, lithostatic stress −1 kb, and hydrothermal fluid pressure −0.9 kb). EO and EO′ represent the possible extent of concentric and radial continuous tension fractures, respectively. B and B′ respectively represent possible extent of concentric and radial brittle faults. RT, CT, RS, and CS denote zones of radial continuous tension fractures, concentric continuous tension fractures, radial brittle faults, and concentric brittle faults. The initial symbols (such as RT·CT) denote the predominant mode of fractures. The unit of scale is arbitrary.

A. Nearly spherical magma reservoir of aspect ratio 1:1.4.
B. Vertically elongated magma reservoir of aspect ratio 1:100.

RT·CT and RT·CS (Fig. 4). Concentric (generally continuous) tension fractures also occur perpendicular to the direction of maximum stress σ_1 (i.e., normal to the plane of figure), in the region of RT·CT (Fig. 2). In this region radial tension fractures are formed prior to concentric fractures, as the stress σ_γ (normal to the plane of figure) is larger than the stress σ_1. As a result, radial tensile fractures predominate, while arcuate, segmented concentric fractures occur in the restricted region of RT·CT (Fig. 5) without forming complete rings. In the region RT·CS, concentric brittle faults also occur along with predominant radial tensile fractures. However, in region RS only radial brittle faults occur. Radial brittle faults are generally oriented at 30° to 45° to the radial plane, while the concentric brittle faults are perpendicular to the radial plane. In natural cases these orientations could, however, vary to some extent, depending upon the rock's inhomogeneity and other physical properties. It is to be noted that no ductile faults occur under such conditions.

The zonal distributions of fracture patterns around a vertically elongated magma body (i.e., of the aspect ratio 1:10 or 1:100) are more complicated than those around a near-spherical magma chamber. For a vertically elongated magma body, the probable fractures, occurring in sequence in the upper part from the walls to the outside of the reservoir, are RT·CT, RT·CS, RS·CS, and RS, respectively (Fig. 4B). This sequence is similar to that around a near-spherical magma body. However, in the lower part of the elongated magma reservoir, only radial tension fractures (RT) appear instead of RS·CS. Ductile faults may also occur outside of RS or CS regions in the lower part. However, the region of ductile faults hardly appears in Figure 4B. The narrow region of RT·CT would extend downward along the walls of the magma reservoir where magma pressure is equivalent to effective interstitial fluid pressure near the walls. Unlike the case of a near-spherical magma reservoir, concentric fractures here predominate in regions CT·RT and CS·RS and in a narrow region of CT·RS and CS above the magma reservoir (Fig. 4). This is due to higher magnitude of maximum stress σ_1 (within the radial plane) over σ_γ (acting normal to the radial plane) inside a funnel-shaped surface (C.F.) (Fig. 3B). The tension fractures inside the funnel-shaped fracture surface (C.F.) are near-vertical, as σ_2 direction is almost vertical. The boundary line EO, on which effective stress is zero, denotes a possible extension of continuous tensile fractures. The boundary line B indicates the possible extent of brittle shear fracture, as the ratio of shearing stress (τ/σ) to

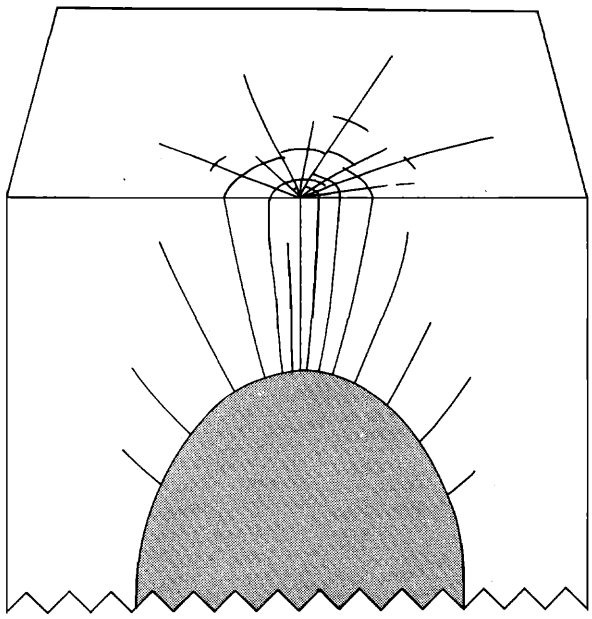

FIG. 5. Possible fracture pattern around a near-spherical prolate magma reservoir due to magma pressure higher than lithostatic stress.

effective normal stress reaches a critical value. If the ratio P/σ_1 for magma reservoir pressure to lithostatic stress and the ratio p/σ_1 for interstitial fluid pressure to lithostatic stress (Eq. 5 and 6) remains the same, it is to be noted that the positions of boundary lines of EO (tensile fractures) and B (brittle shear fractures) would be the same. The position of the funnel-shaped surface (C.F.) will be unaffected by stress conditions, as it is controlled by the apical shape of the magma reservoir. The formation of ductile faults under high interstitial fluid pressure is negligible.

If the interstitial fluid and magma pressures are relatively small compared to the lithostatic stress, the area of brittle fractures around the vertically elongated magma reservoir does not extend far enough to reach the funnel-shaped surface (C.F.) at the top of the magma reservoir. As a result, the predominant fracture patterns are radial fractures accompanying a few segmented concentric fractures, similar to near-spherical magma body (Fig. 6A). If, however, magma and interstitial fluid pressures become large compared to lithostatic stress, the zone of brittle fractures then extends toward the funnel-shaped fracture surface (Fig. 4B). This results in the formation of tensile fractures vertically upward from the apical end of the magma reservoir, as well as in lateral directions. If such tensile fractures reach far enough upward into the funnel-shaped surface (C.F.), concentric fractures then predominate over radial fractures. Tensile frac-

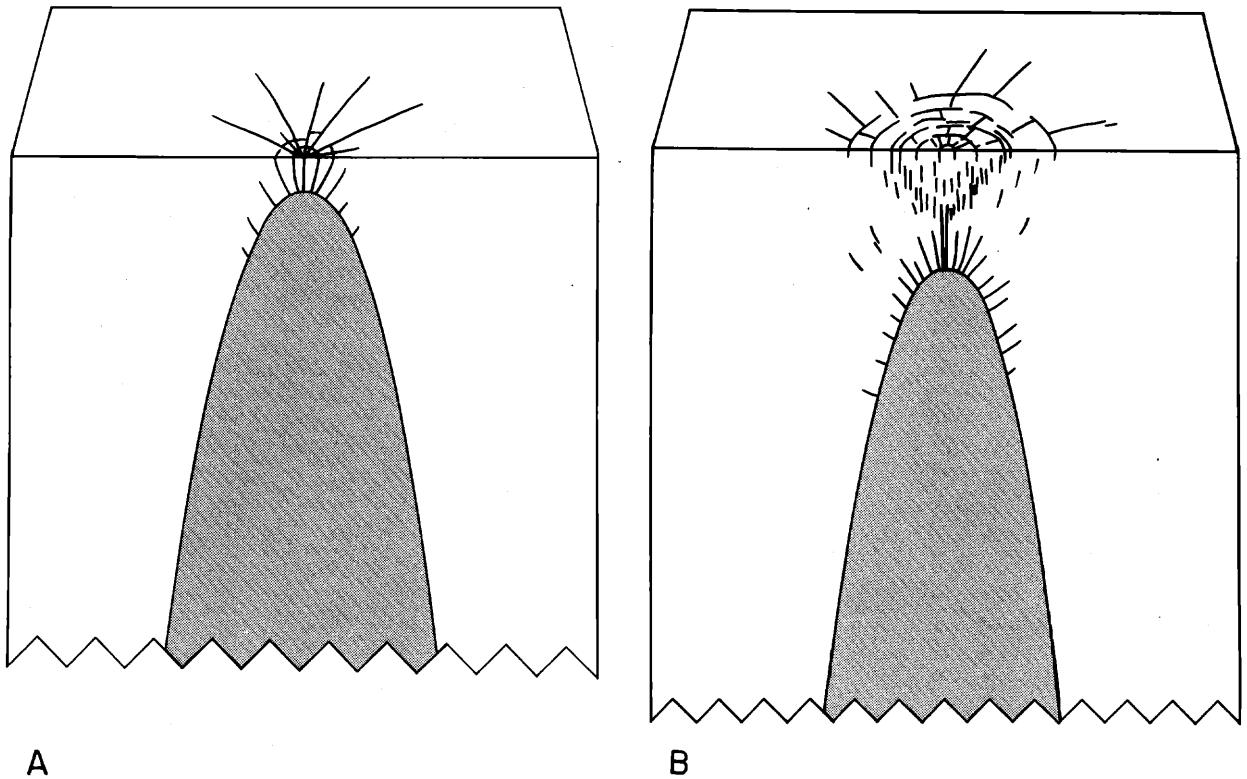

FIG. 6. Possible development of fracture patterns around a vertically elongated prolate magma reservoir due to progressive increase of magma and hydrothermal fluid pressures shown in sequence of A and B.

A. Formation of predominant radial fractures at an initial phase of intrusion when magma and hydrothermal fluid pressures are relatively low (but higher than lithostatic stress).

B. Predominant concentric and peripheral radial fracture patterns due to the increase of magma and hydrothermal fluid pressures. Note the formation of funnel-shaped normal faults and en echelon concentric tension fractures.

tures in such cases tend to shift outward and form en echelon concentric tension fractures (Fig. 6B) as stress contours and boundary lines of fractures become flat or concave upward (Figs. 2 to 4). If deformation progresses further, en echelon concentric brittle faulted segments may continue to form complete faulted rings (as appear in plan view). Some faults also appear as funnel-shaped normal faults (Fig. 6B). For bodies of aspect ratios 1:100 and 1:10, the computed dips of funnel-shaped normal faults above the magma reservoirs appear to be 50° and 60°, respectively (Fig. 2), although the general range of dips may vary between 45° to 60°. Displacement along the normal faults in the central region of the funnel-shaped fracture zone (immediately above the apex of the magma reservoir) may produce some subsidence compared to the peripheral region. It is interesting to note that the distribution of elastic displacement indicates wide domal uplift above magma intrusion, but an area of relative subsidence commonly occurs in the center of the domal uplift, as indicated from our theoretical analyses (Bhattacharji and Koide, in prep.). The formation of central graben in a domal uplift, as observed in many areas of recent magmatic activities, or underground caldera subsidence above deepseated magma rise (intrusion) are also indicated by the existence of vertical extensional stress above a vertically elongated magma reservoir (Fig. 2) from our analyses.

At shallower depths, the lithostatic load is relatively less. As a result, the zone of fractures extends upward and outward. For an elongated magma body intruded at a shallow depth (i.e., closer to the surface), the general distribution of fracture patterns will still be similar, as shown in Figure 4.

Discussion

We have shown from our theoretical analyses, with a three-dimensional solution of elasticity and using the criteria of fracturing of rocks, the conditions and regions of formation of (1) dominant radial fractures, (2) dominant concentric fractures, or combination of radial and concentric fractures,

and (3) conditions for formation of central subsidence (or graben) in a domal uplift related to intrusions of magma bodies of various aspect ratios. Wisser (1960) has given many examples of ore deposits associated with such fracture systems in the North American Cordillera. We will discuss here only a few typical examples of ore-bearing fracture systems whose origin can be correlated with magmatic intrusion(s) at depth.

The system of radial and concentric fractures, faults, and dikes around Silverton cauldron, San Juan Mountains, Colorado, is in good agreement with the predicted fracture patterns above a vertically elongated magma reservoir (Fig. 7). The circular block of Silverton cauldron shows subsidence of 300 to 800 m along closely spaced vertical to steeply inward-dipping formal faults composing the ring fault zone (Burbank and Luedke, 1968). Radial fractures predominate outside the rim of the ring fault zone, and many radial fractures are actually dikes. Most of the productive veins of silver-gold-lead-zinc ore occupy tension fractures radial to the cauldron rim (Burbank and Luedke, 1968). Some veins follow the wall(s) of dikes, while some others occupy both diagonal and concentric fractures. Higher temperature minerals were deposited closest to the rim ring fault zone which seems to have been the trunk channel for ore solutions (Wisser, 1960, p. 35). The cauldron rim fault zone is intruded in some places with large numbers of siliceous volcanic intrusives. Wisser (1960) considered that the Silverton fracture pattern owed its origin to broad doming. Our analyses suggest that the origin of ore-bearing

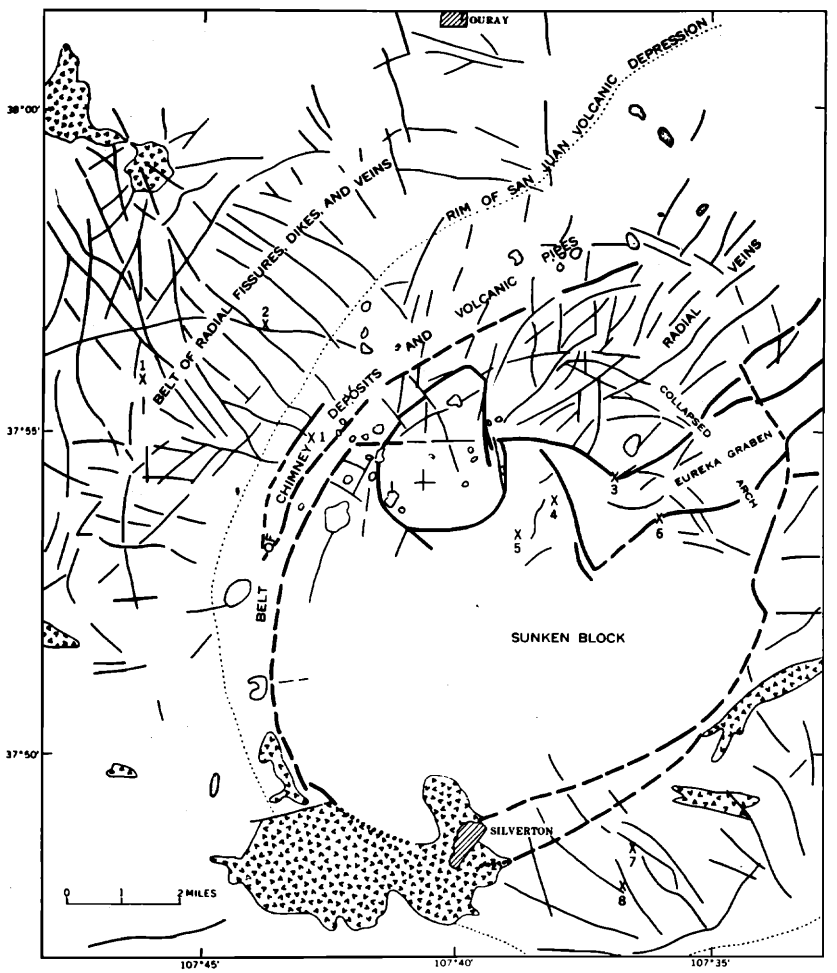

FIG. 7. Fracture patterns around Silverton cauldron, Colorado (after Burbank and Luedke, 1968). Note the similarities of these fracture patterns to the predicted fracture patterns due to an elongated prolate magma body at depth (Fig. 6B). Central block bounded by ring fault zone (heavy lines) shows subsidence and radial dikes and veins (light lines) predominant at the margin. Larger intrusive bodies and volcanic pipes outcrop in the periphery of the ring fault zones.

Silverton fracture patterns is directly related to the wedging of vertically elongated magmatic intrusion rather than to broad doming. Continuous tension fractures, which contain veins or dikes, indicate that their formation is related to high magmatic and interstitial fluid pressures. It appears that there was sufficiently high pressure to keep the fractures open for the deposition of vein minerals. The Silverton cauldron is connected by the Eureka graben zone with the Lake City cauldron, which also has ore-bearing veins in the periphery of its rim fault zone. The occurrence of graben suggests a close relation of both cupolas. The total diameter of 16 km for both Silverton and Lake City caldera suggests the presence (existence) of the top of cupolas at a depth of about 8 km. Radial veins and dikes, as observed around some small intrusives near the Silverton cauldron (Burbank and Luedke, 1968) are, according to our analyses, originally radial fractures now forming veins and dikes around small spheroidal "secondary" magma reservoirs. Alternatively, they may have formed at the flank of small cupolas.

Most important mineralized areas in the central San Juan Mountains, Colorado, are also associated with the latest subsidence structure in a large volcanic caldera complex (Steven, 1968). Regional gravity studies suggest the presence of a concealed batholith genetically related to a near-surface caldera complex now underlying much of the area covered by volcanic rocks (Plouff and Pakiser, 1972). The depth to the top of the batholith ranges from less than 2 km to 7 km beneath the surface. In the Sunlight mining district, Wyoming (Parsons, 1937), predominant radial fractures accompany discontinuous concentric fractures. Many mineralized veins filled reopened older radial and concentric fractures and dikes, caused by slight, continued, or resumed uprise of magma (Wisser, 1960). Such fracture patterns filled by vein minerals and their relation to spheroidal bodies at different depths are predicted from our theoretical analyses.

According to our analyses and interpretation, the caldera subsidence and dominant concentric fractures, such as in the San Juan Mountains, are related to intrusion(s) of vertically elongated magma cupolas and high magma and hydrothermal fluid pressures. Thus, our interpretation differs from Anderson's original contention (1936) that caldera subsidence and outwardly dipping ring fractures result from magma reservoir pressure being lower than lithostatic pressure. Our interpretations are in accord with Billings' (1943, 1945) conclusion from his study of ring dikes in New Hampshire that initial ring fractures are essentially vertical tension fractures due to the upward pressure of magma. Although the block inside the ring fracture may subside, this does not necessarily mean lower magma pressure. Our analysis suggests that ring dikes are formed by magma wedging into (almost) vertical concentric fractures above the vertically elongated cupola under high magma pressures. Cone sheets in the central part are formed by magma occupying a funnel-shaped normal fault zone above the cupola. However, some cone sheets may form by magma filling in low-angle tension fractures in the peripheral region(s) (Figs. 5 and 6).

A recent study of resurgent cauldrons (Smith and Bailey, 1968) suggests that regional tumescence and the propagation of ring and radial fractures with possible apical graben subsidence occurred at the first stage of the resurgent cauldron cycle. Ring fracture volcanism is prominent in both the beginning and later stages of resurgent doming. Smith and Bailey (1968) suggest that there is evidence of cauldron formation in some central vent volcanoes, and that concentric fractures existed prior to subsidence. Such observations and interpretations are in accord with our analyses. We suggest that underground cauldron subsidence occurs along funnel-shaped normal faults (Fig. 6B) above the vertically elongated magma cupola under higher magma and interstitial hydrothermal fluid pressures compared to lithostatic pressure. If funnel-shaped normal faults reach to the surface, surface cauldron subsidence will also occur. According to our interpretation, subsidence is caused primarily by lateral stretching (i.e., spreading or widening) of the underlying main magma reservoir. Later cauldron subsidence can occur due to reduction of magma pressure. Such subsidence generally occurs along fractures formed previously by excess magma pressure. If mafic (basaltic) magmas intrude into a funnel-shaped underground subsidence chamber, funnel-shaped magma bodies are formed, which may act as "secondary" sources for basalts in the crust, and with in situ crystallization and differentiation, can later form stratiform layered intrusion (Bhattacharji and Koide, 1974). If a felsic magma intrudes in such a subsided chamber close to the surface, it may act as a large "secondary" pool in the crust for rhyolite volcanism and/or as a source material for many mineral deposits associated with felsic (rhyolitic) rock (Bhattacharji and Koide, in prep.). It is interesting to note that a large number of copper veins are located in and around such a funnle-shaped rhyolitic body in the Ashio mine, Japan (Imai et al., 1975, fig. 27). These deposits may be genetically related to late Cretaceous or early

Tertiary granitic rock which may exist as a cryptobatholith underneath the funnel-shaped rhyolitic body (Imai, 1966). In the Ashio mine (Imai et al., 1975, Figs. 30, 31), an arcuate brecciated normal fault zone also exists almost parallel to the periphery of a funnel-shaped rhyolitic body. This fault zone is partly mineralized, and replacement orebodies also occur in chert beds. It appears that the arcuate brecciated fault zone is a remnant of original funnel-shaped normal faults. Although the primary mineralization took place during the later phase when the rhyolite was almost solidified, fracturing, subsidence, and early mineralization seem to be related directly to a series of igneous activity. The veins in Ikuno mine, Japan, also formed in a rhyolitic body which occupied an area of probable caldera subsidence (Imai, 1966). The famous veins in Cripple Creek mining district, Colorado (Lindgren, 1928; Lovering and Goddard, 1950), the veins of Potosi mine, Bolivia (Bateman, 1951, p. 470), etc., are also situated in and around funnel-shaped breccia or rhyolitic bodies.

As we pointed out earlier, stress will be axially symmetric along the central axis of the prolate magma body and along the funnel-shaped fracture surface (C.F. Fig. 3), because maximum principal stress (σ_1), acting in the radial direction, is always equal to perpendicular maximum stress σ_γ. Under such an axial-symmetric stress condition, fractures may occur in various directions, and breccia pipes may form along the central axis or along the funnel-shaped surface (C.F.) at the periphery of the funnel-shaped normal fault zone above the vertically elongated magma reservoir (Fig. 8). Chimney deposits and breccia pipes (Fig. 7) are situated in the periphery of the rim fault zone of the Silverton cauldron (Burbank and Luedke, 1968), while Cresson "blow out" in Cripple Creek mining district, Colorado (Loughlin, 1927; Lovering and Goddard, 1950), breccia pipe deposits in Tsuchihata mine, Japan (Imai, 1966), etc., all seem to be central-type breccia pipes. Their origin appears to be directly related to the axial-symmetric stress condition produced by vertically elongated magma chamber(s) at depth.

Many fracture patterns around stock, dome, or areas of caldera subsidence, however, are not always axial symmetric. A symmetric shape of magma body, anisotropic horizontal tectonic stress, anisotropy of the country rocks, etc., can cause the fracture patterns to become asymmetric. The nature of fracture patterns due to anisotropic stress or due to a magma body with elliptical shape (in plan view), are the subjects of future study.

It is important to note that the types of zoning

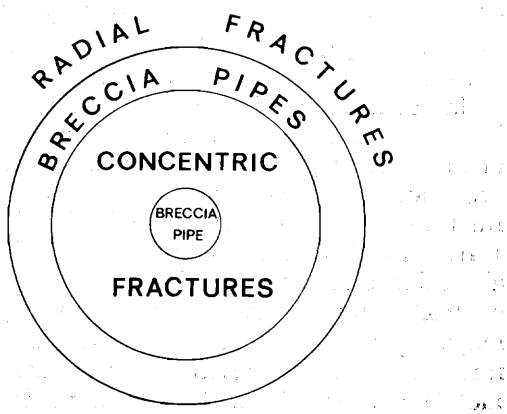

FIG. 8. Diagrammatic sketch of the horizontal zonal distribution of fractures above a vertically elongated prolate magma reservoir. Note the sequence of zones of pipe, concentric, and radial fractures from the axis outward.

of fractures (namely, continuous tension fracture zone, brittle fracture zone, and no fault zone) would largely control the temperature gradient, outward flow of hydrothermal fluids, and the resultant chemical zoning and alteration. The types of fractures, mineral and hydrothermal zoning as observed in Climax molybdenum deposit (Wallace et al., 1968) can be explained from our predicted zoning of fractures as a result of intrusions of elongated magma body. Similar zonings of hydrothermal alteration around a central stock are also observed in many porphyry copper deposits (Sillitoe, 1973).

Interestingly, concentric, radial, and central graben, around a vertically elongated magmatic intrusion, that are predicted from our analysis are also found around diapiric intrusions of viscous or plastic salt or similar materials (Parker and McDowell, 1955; Holmes, 1965).

Conclusions

Stress distribution obtained from an exact solution of three-dimensional theory of elasticity in an infinite elastic rock medium around isolated spheroidal magma reservoirs of various aspect ratios provides the basis for the interpretation of the origin and nature of distributions of ore-bearing fracture systems around magmatic bodies.

The estimation of the stress condition indicates development of possible zonal distribution of fractures from the wall of the magma reservoir outward, in sequence of (1) continuous tension fracture zone, (2) brittle fault zone, and (3) no fault zone. Continuous tension fractures occur under effective tensile stress ($\sigma - p > 0$). Brittle faults, which contain many tension fractures and open shear fractures within the fault zones, occur

when shearing stress overcomes internal friction ($\tau > \mu(\sigma - p)$). Ductile faults, which are essentially unopen fractures between a brittle fault and no fault zone, are unimportant as far as ore mineral localization is concerned. These zonal distributions of fractures suggest, in a general way, the mode of origin and possible extent of distribution of various fracture zones. Hydrothermal fluids which penetrate through fractures and produce hydrothermal alteration and ore mineral deposition are largely controlled by the type(s) of fracturing. While magma can intrude into wide, continuous, tensile fractures or large, brittle fracture zone, highly mobile, low-viscosity hydrothermal fluids can more readily penetrate into brittle fault zone. Hence, brittle fault zone generally is a profitable site for ore localization. Climax molybdenum deposits offer an excellent field example of such zonal distribution of ore-bearing fracture systems and their hydrothermal alterations.

Radial and concentric fracture systems occur around prolate magma reservoirs. When excess magma reservoir pressure exceeds lithostatic pressure, radial fractures are predominant around a near-spheroidal magma body, or immediately above the apex of the vertically elongated magma reservoir or at its flank. Concentric fractures, on the other hand, predominate in the funnel-shaped region above a vertically elongated magma body. They are most likely to form under high magma and hydrothermal fluid pressures. A central graben bounded by funnel-shaped normal faults on wide domal uplifts is formed by the wedging action of magma immediately above the vertically elongated prolate magma reservoir. Near-vertical concentric fractures are formed in the central graben that are generally filled by ring dikes. Cone sheets, in our interpretation, occupy brittle shear faults in the central area and some tension fractures at the periphery of the magma reservoir. A long central graben is generally formed above a vertically elongated, elliptical magma reservoir. Displacement along funnel-shaped normal faults causes underground caldera subsidence at depth above the magma reservoir. If such normal faults extend close to the surface and displacement occurs, surface caldera subsidence can also take place. Breccia pipes may form along the central axis of a prolate magma reservoir or along the boundaries of predominantly concentric and radial fracture zones. Typical fracture patterns accompany cauldron subsidence and are bounded by ring fault zone, and the occurrence of breccia pipe zone at the boundary of the concentric and radial fracture zones in Silverton Cauldron, Colorado, and in other areas, can be explained from our predicted model. Vein-type deposits commonly associated with funnel-shaped felsic (rhyolitic) bodies are related to near-surface caldera subsidence.

Acknowledgments

The authors wish to thank Prof. H. Imai of the University of Tokyo for encouragement and his deep interest in the application of theoretical solution(s) to the problems of ore deposits. The authors are grateful to Dr. A. Sasaki of the Geological Survey of Japan, and to the Science and Technology Agency of the Government of Japan, for making this joint collaboration possible. The work on experimental rock deformation and the theory of fracturing of rocks was done by the senior author at the Geological Survey of Japan. The remainder of this study was financially supported by a grant (GA 24078) from the U. S. National Science Foundation to the second author (S. B.), which allowed the first author to stay in the U. S. A. and made the collaboration possible. The authors are grateful to Brooklyn College of the City University of New York for providing computer facilities and acting as host for the senior author, and particularly to Dr. M. Gabriel, Dean of the School of Science, for providing additional funds for completion of this research. We thank Mrs. M. Dugan for typing the manuscript and J. Kelberman for drafting the figures.

DEPARTMENT OF GEOLOGY
BROOKLYN COLLEGE OF THE
CITY UNIVERSITY OF NEW YORK
BROOKLYN, NEW YORK 11210

H. K., PRESENT ADDRESS:
GEOLOGICAL SURVEY OF JAPAN
8 KAWADA-CHO, SHINJUKU-KU
TOKYO, JAPAN

REFERENCES

Anderson, E. M., 1936, The dynamics of the formation of cone sheets, ring-dykes and cauldron subsidences: Royal Soc. Edinburgh Proc., v. 56, p. 128–157.

—— 1938, The dynamics of sheet intrusion: Royal Soc. Edinburgh Proc., v. 58, p. 242–251.

—— 1951, The dynamics of faulting, 2d ed.: Edinburgh, Oliver and Boyd, 206 p.

Aramaki, S., 1971, Hydrothermal determination of temperature and water pressure of the magma of Aira caldera, Japan: Am. Mineralogist, v. 56, p. 1760–1768.

Bateman, A. M., 1951, Economic mineral deposits, 2d ed.: New York, John Wiley & Sons, 916 p.

Bhattacharji, S., and Koide, H., 1974, Fracturing in lithospheric plates by magma induced pressure [abs.]: Eos (Am. Geophys. Union Trans.), v. 55, p. 439.

Bhattacharji, S., and Schleifer, S., 1970, Mechanics of stoping and stope melting by natural thermal convection in cylindrical neck: Am. Geophys. Union Trans., v. 51, p. 830.

Billings, M. P., 1943, Ring-dikes and their origin: N. Y. Acad. Sci. Trans., ser. 2, v. 5, p. 131–144.

—— 1945, Mechanics of igneous intrusion in New Hampshire: Am. Jour. Sci., v. 243A, p. 41–68.

Burbank, W. S., and Luedke, R. G., 1968, Geology and ore deposits of the western San Juan Mountains, Colorado, *in* Ridge, J. E., ed., Ore deposits of the United States, 1933–1967: New York, Am. Inst. Mining Engineers, p. 714–733.

Durrance, E. M., 1967, Photo-elastic stress studies and their application to a mechanical analysis of the Tertiary ring-complex of Ardnamurchan, Argyllshire: Geologists' Assoc. London Proc., v. 78, p. 289–318.

Edwards, R. H., 1951, Stress concentrations around spheroidal inclusions and cavities: Jour. Applied Mechanics, v. 18, p. 19–30.

Emmons, W. H., 1933, On the mechanism of the deposition of certain metalliferous lode systems associated with granitic batholiths, *in* Ore deposits of the Western States: New York, Am. Inst. Mining Engineers, p. 327–349.

—— 1937, Gold deposits of the world: New York, McGraw Hill Book Company, 562 p.

—— The principles of economic geology, 2nd ed.: New York, McGraw-Hill Book Company, 562 p.

Garson, M. S., 1959, Stress pattern of carbonatitic and alkaline dykes at Tondulu ring structure, southern Nyasaland: Internat. Geol. Cong., 20th, Mexico 1956, Asoc. Serv. Geol. Africanos, Actas y Trabajos, p. 309–323.

Gilluly, J., 1946, The Ajo mining district, Ariz.: U. S. Geol. Survey Prof. Paper 209, 112 p.

Griffith, A. A., 1925, The theory of rupture: Internat. Cong. Applied Mechanics, 1st, Delft, Proc., p. 53–63.

Handin, J., Hager, R. V., Jr., Friedman, M., and Feather, J. N., 1963, Experimental deformation of sedimentary rocks under confining pressure: pore pressure tests: Am. Assoc. Petroleum Geologists Bull., v. 47, p. 717–755.

Hast, N., 1973, Global measurements of absolute stress: Royal Soc. London Philos. Trans., A, v. 274, p. 409–419.

Holmes, A., 1965, Principles of physical geology, 2d ed.: New York, The Ronald Press Company, 1288 p.

Hubbert, M. K., and Rubey, W. W., 1959, Role of fluid pressure in mechanics of overthrust faulting, Part I: Geol. Soc. America Bull., v. 70, p. 115–166.

Imai, H., 1966, Formation of fissures and their mineralization in the vein-type deposits of Japan: Univ. Tokyo Fac. Engineering Jour. (B), v. 28, p. 255–302.

——Lee, M. S., Iida, K., Fujiki, Y., and Takenouchi, S., 1975, Geologic structure and mineralization of the xenothermal vein-type deposits in Japan: Econ. Geol., v. 70, p. 647–676.

Ishihara, S., 1967, Molybdenum mineralization at Questa mine, New Mexico, U. S. A.: Japan Geol. Survey Rept. 218, p. 1–64.

Koide, H., 1968, A tectonophysical study of the initiation and development of fracture in rocks: Ph.D. thesis, University of Tokyo.

—— 1970, Condition for fracture formation from inclusion. I, Soft inclusion and pore: Mat. Sci. Soc. Japan Jour., v. 7, p. 252–263.

—— 1971, Fractures aligned en echelon and fracture patterns: Soc. Mining Geologists Japan Spec. Issue 3 (IMA-IAGOD Meetings '70 Proc., IAGOD vol.), p. 107–114.

—— 1972, Fracture initiation in brittle polycrystalline material such as rocks, *in* Mechanical behavior of materials: Internat. Conf. on Mechanical Behavior of Materials, 1971, v. 4, p. 455–463.

—— 1974, Fractures and their relation to the generation of magma in the depth, *in* Fracturing and igneous activity: Assoc. Geol. Collaboration Japan Mon. 18, p. 87–90 (in Japanese).

—— Hoshino, K. and Inami, K., 1974, Fault models based on an extended Griffith's theory: Japan Geol. Survey Bull., v. 25, p. 89–103 (in Japanese).

Lindgren, W., 1928, Mineral deposits, 3rd ed.: New York, McGraw-Hill Book Company, 1049 p.

Loughlin, G. F., 1927, Ore at deep levels in the Cripple Creek district: AIME Trans., v. 75, p. 42–73.

Lovering, T. S., and Goddard, E. N., 1950, Cripple Creek district, *in* Geology and ore deposits of the Front Range, Colorado: U. S. Geol. Survey Prof. Paper 625-A, p. A1–A17.

Mogi, K., 1974, Volcanoes and cracks in deep regions, *in* Fracturing and igneous activity: Assoc. Geol. Collaboration Japan Mon. 18, p. 83–85 (in Japanese).

Newhouse, W. H., ed., 1942, Ore deposits as related to structural features: Princeton, Princeton Univ. Press, 280 p.

Odé, H., 1957, Mechanical analysis of the dike pattern of the Spanish Peaks area, Colorado: Geol. Soc. America Bull., v. 68, p. 567–576.

Onda, I., 1960, The formation of the caldera of the Krakatoa type with reference to earth's crust elasticity: Hokkaido Univ. Geophys. Bull., v. 7, p. 77–88. (in Japanese)

Parker, T. J., and McDowell, A. N., 1955, Model studies of salt-dome tectonics: Am. Assoc. Petroleum Geologists Bull., v. 39, p. 2384–2470.

Parsons, W. H., 1937, The ore deposits of the Sunlight region, Park Co., Wyoming: Econ Geol., v. 32, p. 832–854.

Plouff, D., and Pakiser, L. C., 1972, Gravity study of the San Juan mountains, Colorado: U. S. Geol. Survey Prof. Paper 800-B, p. B183–190.

Ridge, J. D., 1968, Changes and developments in concepts of ore genesis—1933 to 1967, *in* Ridge, J. D., ed., Ore deposits of the United States, 1933–1967: New York, Am. Inst. Mining Engineers, p. 1713–1834.

Roberts, J. L., 1970, The intrusion of magma into brittle rocks, *in* Newall, G., and Rast, N., eds., Mechanism of igneous intrusion: London, Gallery Press, p. 287–338.

—— 1972, The mechanics of overthrust faulting, a critical review: Internat. Geol. Cong., 24th, Montreal 1972, sec. 3, p. 593–598.

Robson, G. R., and Barr, K. G., 1964, The effect of stress on faulting and minor intrusions in the vicinity of the magma body: Bull. volcanol., v. 27, p. 315–330.

Sadowski, M. A., and Sternberg, E., 1947, Stress concentration around an ellipsoidal cavity in an infinite body under arbitrary plane stress perpendicular to the axis of the cavity: Jour. Applied Mechanics, v. 69, p. 191–201.

—— 1949, Stress concentration around a triaxial ellipsoidal cavity: Jour. Applied Mechanics, v. 71, p. 149–157.

Sheppard, S. M. F., Nielsen, R. L. and Taylor, H. P. Jr., 1969, Oxygen and hydrogen isotope ratios of clay minerals from porphyry copper deposits: Econ. Geol., v. 64, p. 755–777.

Sillitoe, R. H., 1973, The tops and bottoms of porphyry copper deposits: Econ. Geol., v. 68, p. 799–815.

Smith, R. L., and Bailey, R. A., 1968, Resurgent cauldrons, *in* Coats, R. R., Hay, R. L., and Anderson, C. A., eds., Studies in volcanology: Geol. Soc. America Mem. 116, p. 613–662.

Steven, T. A., 1968, Ore deposits in the central San Juan mountains, Colorado, *in* Ridge, J. D., ed., Ore deposits in the United States, 1933–1967: New York, Am. Inst. Mining Engineers, p. 706–713.

Suzuki, K., Nishimatsu, Y., and Ishijima, Y., 1967, Measurement of absolute stresses in rock and its interpretation in terms of viscoelastic theory (Part 1): Mining Metall. Inst. Japan Jour., v. 83, p. 793–799.

Taylor, H. P. Jr., 1971, Oxygen isotope evidence for large-scale interaction between meteoric ground waters on Tertiary granodiorite intrusions, Western Cascade Range, Oregon: Jour. Geophys. Research, v. 76, p. 7855–7874.

Wallace, S. R., Muncaster, N. K., Jonson, D. C., Mackenzie, W. B., Bookstrom, A. A., and Surface, V. E., 1968, Multiple intrusion and mineralization at Climax, Colorado, *in* Ridge, J. D., ed., Ore deposits of the United States, 1933–1967: New York, Am. Inst. Mining Engineers, p. 605–640.

White, D. E., 1968, Environment of generation of some base-metal ore deposits: Econ. Geol., v. 63, p. 301–335.

Wisser, E., 1960, Relation of ore deposition to doming in the North American Cordillera: Geol. Soc. America Mem. 77, 117 p.

Yokoyama, I., 1971, A model of the crustal deformations around volcanoes: Jour. Physics Earth, v. 91, p. 199–207.

—— 1974, Calderas and their formation, *in* Fracturing and igneous activity: Assoc. Geol. Collaboration Japan Mon. 18, p. 40–53.